Acoustic Resonator Tuning Strategies for the Narrowband Noise Control in an Enclosure

Zhongyu HU[a], Cheng YANG[a,b] and Li CHENG[a*]

[a] Department of Mechanical Engineering, The Hong Kong Polytechnic University

[b] Institute of Vibration, Shock and Noise, School of Mechanical Engineering, Shanghai Jiao Tong University, Shanghai, China

[*]Corresponding author, e-mail: li.cheng@polyu.edu.hk,

Abstract

The tuning of an acoustic resonator, in terms of its Helmholtz frequency and the internal resistance, is investigated for the control of a narrowband noise in an acoustic enclosure. This paper extends our previous work on the resonance control to a more general scenario in which the noise generated may be either close to, far away from, or in-between the resonance frequencies of the enclosure. Based on a theoretical model, energy radiation and dissipation of the resonator and its interaction with the acoustic enclosure are scrutinized. Numerical studies show the possibility of using mistuned resonators to maximize the noise reduction, as well as the tuning level required for different narrow frequency bands of interests. The effects of the internal resistance of the resonators as well as its dominance levels in the energy dissipation process are also demonstrated. Part of the numerical findings are validated through experiments.

Keywords: *acoustic resonator; mistuned resonator; acoustic energy reduction; internal resistance.*

1. Introduction

Researches on Helmholtz resonators (HRs) have been conducted for over a century since Helmholtz first developed the theory on acoustic resonators [1], as evidenced by a large amount of work reported in the literature. As an efficient noise control device, HR has been extensively used in various systems such as double panels [2-4], small enclosures [5-9] and cylindrical shells [10]. In such applications, HRs are mainly used to suppress the lower-order system resonances which are difficult to deal with using classical sound absorption materials. The control performance of the HR, when deployed in an acoustic system, depends not only on the characteristics of the HR itself but also on its coupling with the acoustic modes of the system.

Van Leeuwen [11] conducted an analysis on the damping effect of a HR on the eigen-tones of a small room using an electrical circuit analogy based on the examination of the coupling between one room mode and the HR. Improvement on similar topic was made by Fahy and Scofield [12] using a fully coupled model that accounts for the interaction between multiple modes of an enclosure and a resonator. By assuming that the averaged separation between the resonance frequencies of the enclosure greatly exceeds the average modal bandwidth, the coupling between one enclosure mode and a resonator was studied analytically. It was found that, unlike the case of a resonator coupled to a free space in which the maximum power absorption is determined by the matching between the sound radiation and the internal resistance of the resonator, the maximum power absorption is simply inversely proportional to the internal resistance of the resonator. This is because that the resonator, acting like a secondary source, re-radiates acoustic energy into the enclosure, thus resulting in an effective interaction with the original acoustic field produced by the primary acoustic source. Cummings [13] extended Fahy and Scofield's model to multiple resonators through analyzing the coupling between multiple enclosure modes and a resonator array. In that work, the HRs were assumed to behave like small pulsating spheres and the averaged acoustic pressure on the surface of

each sphere was calculated by avoiding the singularity problem of the point source assumption. However, a relatively large discrepancy was observed between the coupled frequencies obtained from Cummings's pulsating sphere model and those obtained from the measurement, due to the pulsating sphere assumption. This problem was overcome by Li and Cheng [14] by directly solving the fully coupled equation arising from the interaction, inherent in the enclosure-resonator system. Later on, Yu *et al.* [15] used this model to study the working mechanism of a resonator for the control of the enclosure noise within different bandwidths. Analyses show that, for the narrowband noise control, the radiation of the resonator dominates; whereas with the increasing band, the energy dissipation of the resonator becomes important.

The aforementioned work mainly focused on abating noise at or in the vicinity of the resonance frequency of an enclosure. In practice, however, a good design should prevent the system from major resonances, especially at low frequencies. Occasions arise in which noise can be generated within a narrow frequency band, away from any resonance frequency of an enclosure mode. A representative noise source is the rotating machinery which produces noise at its blade passing frequency. In such cases, the extent to which previous resonator design principles can be utilized remains unknown. This motivates the present work, and to that end, the acoustic resonator design strategy is revisited in a broader context to include off-resonance narrowband control based on the tuning of two resonator parameters, i.e. Helmholtz frequency and the internal resistance.

This paper is organized as follows. In Section 2, a theoretical model describing the coupling between one resonator and an enclosure will be recalled. Based on the model, the energy dissipated and radiated by the resonator are separately quantified, and an acoustic energy reduction index is defined to evaluate the control performance. In Section 3, the tuning strategy of the Helmholtz frequency is investigated for both resonance and off-resonance cases. In Section 4, the internal resistance of the resonator is investigated to reveal the working

mechanism of the resonator in different frequency regions, formulating recommendations for choosing proper internal resistance to improve the noise control performance. Experiment validations are then presented in Section 5.

2. Theoretical model

The system under investigation comprises a rigid-walled enclosure and a classical HR, shown in Fig. 1. The HR consists of a cavity volume V^R, a neck of area S^R and effective length l^R. Throughout this paper, the superscripts and subscripts E, R and S indicate variables associated with "enclosure", "resonator" and "source", respectively.
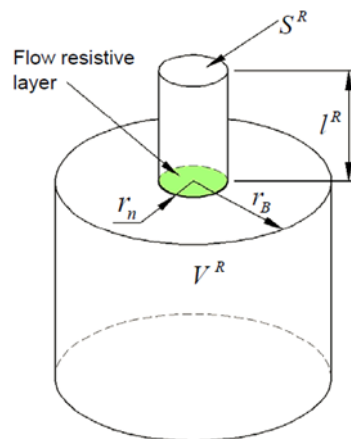

Fig. 1. A damped classical Helmholtz resonator

2.1 Acoustic interaction between an enclosure and one resonator

The acoustic pressure inside the enclosure is governed by the inhomogeneous wave equation [16]

$$\nabla^2 p(\boldsymbol{r},t) - \frac{1}{c^2}\ddot{p}(\boldsymbol{r},t) = -\rho_0 \dot{q}(t)\delta(\boldsymbol{r}-\boldsymbol{r}_0), \tag{1}$$

where $\dot{q}(t)$ is the source volume velocity per unit volume; c is the sound speed; and $\delta(\boldsymbol{r}-\boldsymbol{r}_0)$ is the Dirac delta function. The primary acoustic field inside the enclosure is excited by a harmonic source with q^S located at point $\boldsymbol{r}^S$; while the resonator with an equivalent source volume velocity per unit volume q^R, located at point $\boldsymbol{r}^R$ (center of the resonator orifice), forms

the secondary acoustic source. Using the acoustic impedance of the resonator at its orifice Z [17], q^R is given by $q^R(t) = p(r,t)/Z$. Equation (1) becomes

$$\nabla^2 p(r,t) - \frac{1}{c^2}\ddot{p}(r,t) = -\rho_0 \left[\frac{\dot{p}(r,t)\delta(r-r^R)}{Z} + \dot{q}^S(t)\delta(r-r^S)\right]. \tag{2}$$

The acoustic pressure $p(r,t)$ can be decomposed over the enclosure modes as $p(r,t) = \sum_{j=1}^{J} \Psi_j(t)\varphi_j(r)$, in which $\Psi_j(t)$ is the time-dependent modal response of the jth mode, $\varphi_j(r)$ is the jth eigenfunction and J is the maximum number of the truncated mode series. Assuming all the time dependent variables are harmonic and applying the orthogonality property, the analytical solutions of the velocity of the equivalent volume source $\tilde{Q}^R$ directed outward from the resonator orifice into the enclosure and the jth modal response P_j of the enclosure-resonator system are, respectively,

$$\tilde{Q}^R = \frac{A^R \frac{V^R}{V^E}\sum_{h=1}^{J}\frac{\omega^2}{\omega^2-(\gamma_h^E)^2}\frac{\varphi_h(r^R)}{\Lambda_j}\tilde{\varphi}_h(r^S)\tilde{Q}^S}{1 - A^R \frac{V^R}{V^E}\sum_{h=1}^{J}\frac{\omega^2}{\omega^2-(\gamma_h^E)^2}\frac{\varphi_h^2(r^R)}{\Lambda_h}}, \tag{3}$$

$$P_j = -\frac{iz_0}{kV^E}\frac{\omega^2}{\omega^2-(\gamma_j^E)^2}\frac{\tilde{\varphi}_j(r^S)}{\Lambda_j}\tilde{Q}^S - \frac{iz_0}{kV^E}\frac{\omega^2}{\omega^2-(\gamma_j^E)^2}\frac{\varphi_j(r^R)}{\Lambda_j}\tilde{Q}^R, \tag{4}$$

where

$$A^R = \frac{(\omega^R)^2}{\omega^2 - \frac{i\omega R_i}{\rho_0 L^R} - (\omega^R)^2} ;$$

$\tilde{Q}^S$ is the velocity of the primary volume source, obtained from $q^S(t) = \tilde{Q}^S e^{i\omega t}$; V^E is the volume of the enclosure; γ_j^E is the jth complex eigenvalue of the enclosure expressed as $\gamma_j^E = \omega_j^E + iC_j^E$, in which the real part is the angular frequency and the imaginary part is an equivalent *ad-hoc* damping coefficient; $\Lambda_j = \int_{V^E}[\varphi_j^2(r)]^2 dV/V^E$; $\tilde{\varphi}_j(r^S)$ is the averaged $\varphi_j(r^S)$ over the volume of the primary acoustic source; R_i is the specific acoustic resistance of the resonator; and $\omega^R = c\sqrt{(S^R L^R/V^R)}$ is the Helmholtz frequency of the HR.

Equation (4) provides the analytical solution to the acoustic response of the enclosure in the presence of a single resonator. It implies that the acoustic field comprises two parts: the primary acoustic source field and the secondary acoustic source field. The latter is attributed to the resonator radiation and arises from the coupling between the resonator and multiple enclosure modes. The resistance of the resonator is also an important factor which determines the acoustic interaction. On one hand, it governs the dissipation capability of the vibrating fluid in the neck of the resonator; on the other hand, it affects the extent to which the resonator radiates energy into the enclosure.

2.2 Energy radiation from the resonator

The modal response P_j^R caused by the resonator alone writes

$$P_j^R = \frac{\omega^2}{\omega^2 - (\gamma_j^E)^2} A^R \frac{V^R}{V^E} \frac{\varphi_j(\boldsymbol{r}^R)}{\Lambda_j} \sum_{h=1}^{J} \varphi_h(\boldsymbol{r}^R) P_h, \tag{5}$$

where P_h can be obtained from Eq. (4) by replacing the subscript j with h. The generalized amplitude of the acoustic pressure induced by the resonator radiation can be calculated as

$$\hat{p}(\boldsymbol{r}) = \sum_{j=1}^{J} P_j^R \varphi_j(\boldsymbol{r}). \tag{6}$$

The energy emitted from the resonator orifice in a time period of T can be expressed as

$$E_{radiation}^R = w + w_d, \tag{7}$$

where w is the time-averaged acoustic energy inside the enclosure, including both the potential energy and kinetic energy, and w_d is the time-averaged energy dissipation inside the enclosure, which is approximately determined by the Q-factor of the enclosure Q^E as

$$w_d = \frac{2\pi}{Q^E} w. \tag{8}$$

The time-averaged acoustic energy w over the enclosure volume V is calculated by [15]:

$$w = \int_V \frac{1}{4\rho_0 c^2} \left[\left(\frac{c}{\omega}\right)^2 \nabla \hat{p} \cdot \nabla \hat{p}^* + |\hat{p}|^2 \right] dV \tag{9}$$

in which the two terms in the square bracket are the time-averaged kinetic energy and potential energy, respectively. When the integrated volume V is the entire volume of the enclosure V^E, Eq. (9) writes

$$w = \frac{V^E}{4\rho_0 c^2}\left[\frac{1}{\omega^2}\sum_{j=1}^{J}(\omega_j^E)^2(P_j^R)^2\Lambda_j + \sum_{j=1}^{J}(P_j^R)^2\Lambda_j\right] \tag{10}$$

2.3 Energy dissipation by the resonator

The energy dissipated by the resonator within a period T writes

$$E_d^R = -\frac{1}{2}\int_0^T\int_{S^R}Re[\hat{p}(\boldsymbol{r}^R)\hat{v}^*(\boldsymbol{r}^R)]dSdt. \tag{11}$$

Under the lumped mass assumption, the energy dissipated by the resonator is calculated from

$$E_d^R = -\frac{1}{2}S^R R_i T|\hat{v}(\boldsymbol{r}^R)|^2, \tag{12}$$

in which $|\hat{v}(\boldsymbol{r}^R)|^2$ writes

$$|\hat{v}(\boldsymbol{r}^R)|^2 = \frac{1}{(\rho_0 L^R)^2}\frac{\omega^2}{[(\omega^R)^2 - \omega^2]^2 + \left(\frac{\omega R_i}{\rho_0 L^R}\right)^2}\left|\sum_{h=1}^{J}\varphi_h(\boldsymbol{r}^R)P_h\right|^2. \tag{13}$$

Substituting Eq. (12) into Eq. (11) and replacing T by $2\pi/\omega$ yield

$$E_d^R = \frac{\pi S^R}{\rho_0 L^R}\frac{\frac{\omega R_i}{\rho_0 L^R}}{[(\omega^R)^2 - \omega^2]^2 + \left(\frac{\omega R_i}{\rho_0 L^R}\right)^2}\left|\sum_{h=1}^{J}\varphi_h(\boldsymbol{r}^R)P_h\right|^2. \tag{14}$$

If only the jth enclosure mode is considered, the power dissipated by the resonator at the resonance frequency, i.e. $\omega = \omega^R = \omega_j$, is simplified from Eq. (14) as

$$(P_w)_d^R = \frac{E_d^R}{T} = \frac{S^R}{2R_i}T\left|\varphi_j(\boldsymbol{r}^R)P_j(\omega^R)\right|^2. \tag{15}$$

From Eq. (15), the modal response of the jth enclosure mode can be obtained as

$$\frac{P_j}{\frac{iz_0}{k^R V^E} \tilde{Q}^S} = \frac{\tilde{\varphi}_j(\boldsymbol{r}^S)}{i\Lambda_j^E} \frac{Q_j^E}{1 + Q^R Q_j^E \varepsilon^2}, \tag{16}$$

where k^R is the wave number at the resonance frequency of the jth mode, $Q^R = \omega \rho_0 L^R / R_i$ according to Eq. (16), and $Q_j^E = \omega^R / 2C_j^E$. In the absence of the resonator, the normalized modal response of the enclosure writes

$$\frac{P_j^0}{\frac{iz_0}{k^R V^E} \tilde{Q}^S} = \frac{\tilde{\varphi}_j(\boldsymbol{r}^S)}{i\Lambda_j^E} Q_j^E. \tag{17}$$

Substituting Eq. (16) and (17) into Eq. (15), the power dissipated by the resonator at the resonance frequency of the jth enclosure mode can be obtained as

$$(P_w)_d^R = \frac{S^R}{2\rho_0 c k_j L^R} \left| \frac{Q^R}{1 + Q^R Q^E \varepsilon^2} \right|^2 \left| \hat{P}^{R_0} \right|^2, \tag{18}$$

where $\hat{P}^{R_0}$ is the amplitude of the acoustic pressure at $\boldsymbol{r}^R$ without the resonator. When only one mode is considered, Eq. (18) leads to the same dissipated power expression as the one proposed in Ref. [12].

2.4 Quantifications of the band-averaged performance of the resonator

To quantify the control performance of the resonator over a selected frequency band, an acoustic energy reduction index is defined, which will be used as the parameter to optimize the internal resistance of the resonator. After obtaining the modal response from Eq. (4), the acoustic energy inside the enclosure can be directly calculated from Eq. (10). The averaged acoustic energy within the frequency band $[\omega_1, \omega_2]$ is defined as

$$E^R = \frac{1}{\omega_2 - \omega_1} \int_{\omega_1}^{\omega_2} w d\omega. \tag{19}$$

The frequency band $[\omega_1, \omega_2]$ is usually selected based on the control requirement, which may or may not contain any acoustic resonance of the enclosure. When calculating w by Eq.

(9), the volume V can be either a portion or the entire volume of the enclosure, depending again on the control requirement. The so-called acoustic energy reduction index (ER) is defined as

$$\text{ER} = -10 \log_{10} \frac{E^R}{E^0},\qquad(20)$$

in which E^R and E^0 are the acoustic energy with and without the resonator, respectively.

3. Design strategy of the Helmholtz frequency

In this section, the tuning of the Helmholtz frequency on the reduction of the narrowband noise in an enclosure is investigated. A rectangular enclosure with L_x =976mm, L_y =695mm, L_z =1188mm is used in the calculation. An acoustic monopole source and an observer point are located at (100, 59, 0)mm and (816, 70, 1028)mm, respectively, both being arbitrarily chosen. The number of the enclosure modes considered in the simulation is 216 (6 for each direction), which is proved to be sufficient to ensure the convergence of the calculation result. For the sake of convenience, simulations are conducted for an acoustic source having uniform source strength across the entire frequency spectrum while the narrowband effect of the resonator is accounted for by integrating the system response over a selected frequency region. The Sound Pressure Level (SPL) at the observer point is calculated within a frequency band and shown in Fig. 2, with four resonance frequencies tabulated in Tab. 1.

Table 1. Computed natural frequencies of the enclosure

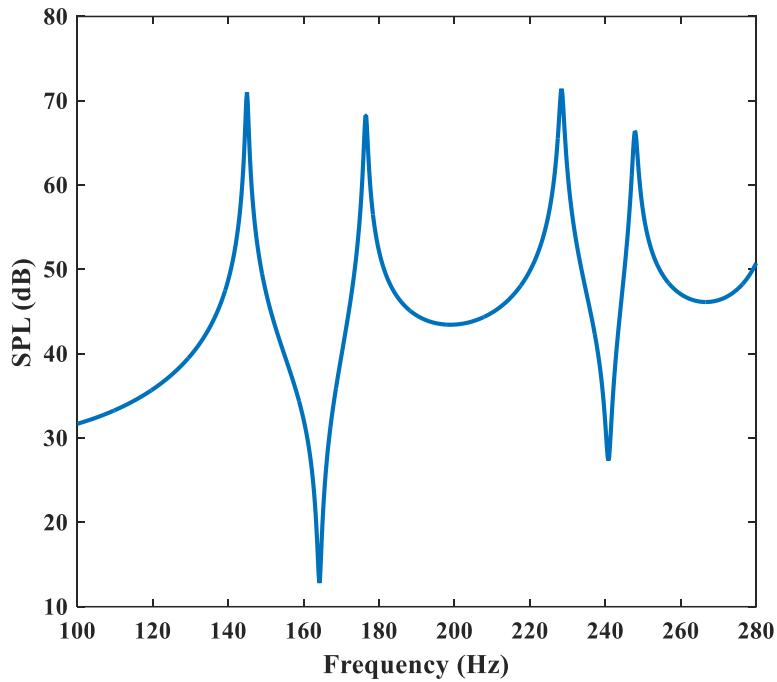| Index	Mode number (lmn)	Natural frequency (Hz)
1	001	145
2	100	176.6
3	101	228.4
4	010	247.8

Fig. 2. Predicted baseline SPL at the observer point (816, 70, 1028)mm.

3.1 Tuned and mistuned resonators

The effect of the Helmholtz frequency of the resonator is first examined on a selected resonance of the enclosure, *e.g.* the second one, within a 3Hz bandwidth centered at 176.6Hz. Two resonators, one tuned exactly to the central frequency of the narrowband (called tuned resonator) and the other off the central frequency (called mistuned resonator), are investigated, respectively. The resultant SPLs are compared with the case without resonator in Fig. 3. It can be seen that both resonators are effective in suppressing the resonance peak of the enclosure, each giving rise to a pair of coupled peaks when the resonators are added. The increase in the SPL due to the coupled peaks is beyond the 3Hz bandwidth. Using Eq. (20), the band-averaged energy reduction for the tuned resonator case is 16dB, which is 2.4dB lower than the mistuned resonator case within the specified frequency band, implying a better performance of the mistuned resonator in this case.
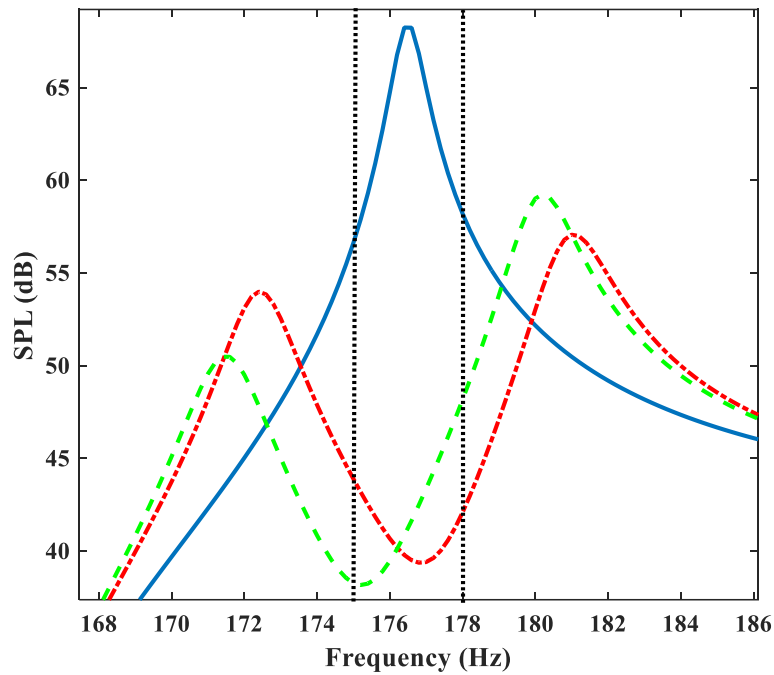
Fig. 3. Control performance of different resonators in the resonance region: —— without resonator; ----- with tuned resonator (176.6Hz); ---·--- with mistuned resonator (178.0Hz)

The advantage of using mistuned resonator in achieving a greater noise reduction within a given narrow frequency band is also found when considering a band away from any of the resonance frequencies of the enclosure. This is evidenced by comparing two different frequency regions: one slightly off the resonance frequency of the enclosure (called transition region); and the other one approximately located in the middle of two neighboring resonance frequencies of the enclosure (called off-resonance region). Again, the control performances using tuned and mistuned resonators are shown in Figs. 4 and 5, respectively. For the transition region, as is shown in Fig. 4, the band-averaged energy reduction brought by the mistuned resonator is 10.1 dB, which is 4.4 dB better than the tuned case. For the off-resonance region, as is shown in Fig. 5, the band-averaged energy reduction of the mistuned resonator is 0.7dB better than that of the tuned one, albeit the rather small reduction produced in both cases (2.2 dB and 2.9 dB, respectively).
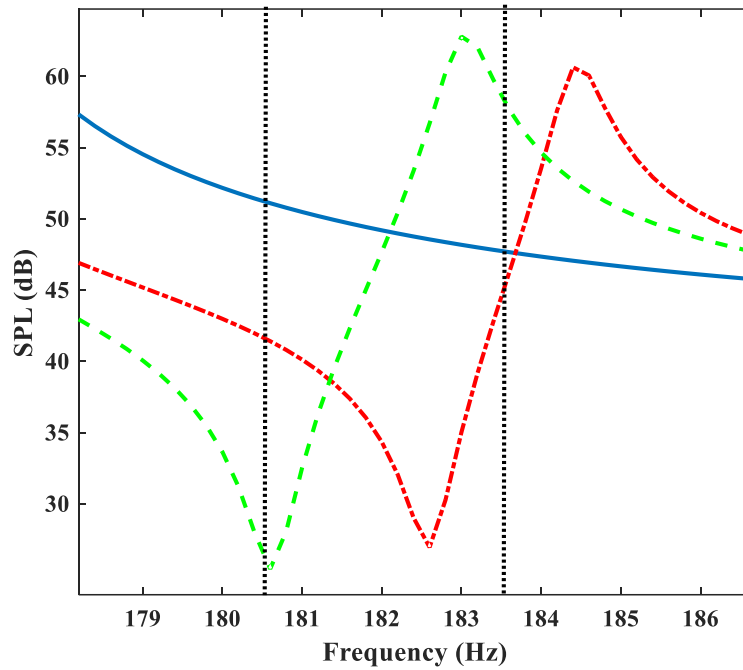
Fig. 4. Sound pressure levels using two different resonators in the transition region: —— without resonator; ----- with tuned resonator (182Hz); ----- with mistuned resonator (184.8Hz)
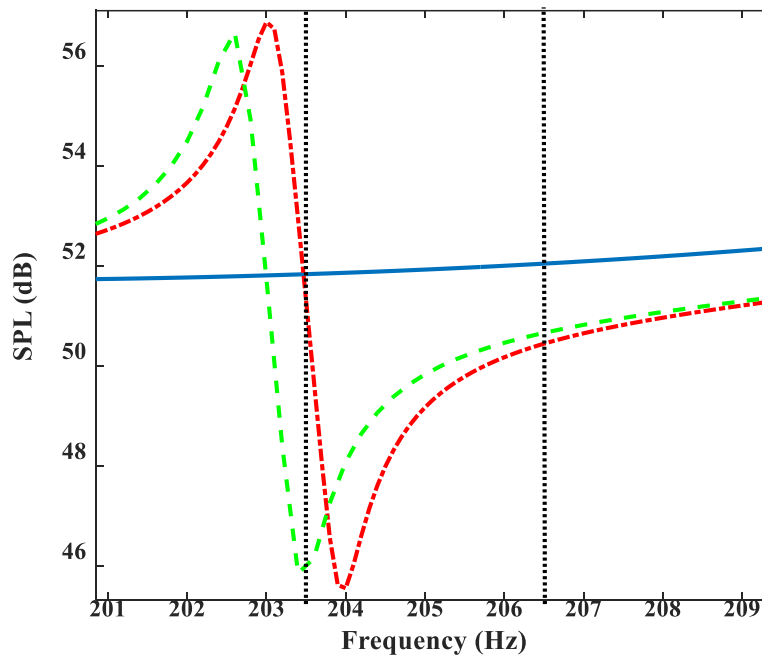

Fig. 5. Sound pressure levels using two different resonators in the off-resonance region: —— without resonator; ----- with critical tuned resonator (205Hz); ------ with mistuned resonator (205.8Hz)

3.2 Mistuning effect of the resonator

The above results imply that a resonator may be mistuned from the central frequency of the narrowband noise to achieve a better noise control performance. To further understand and assess the phenomena observed above, the mistuning effect is examined with the narrowband noise sweeping over a wide frequency range. For each targeted narrowband, a frequency difference is defined as

$$\Delta f = f_{tuned} - f_{optimal} , \tag{21}$$

where f_{tuned} and $f_{optimal}$ are, respectively, the Helmholtz frequency of the tuned resonator and the optimized Helmholtz frequency of the resonator when the maximum band-averaged energy reduction is achieved, which can be either a tuned or mistuned resonator.

Figure 6(a) shows Δf as a function of the central frequency of the narrowband noise, with different line styles representing different bandwidths, namely 3Hz, 5Hz, and 7Hz, respectively. It can be observed in Fig. 6(a) that the variation of Δf exhibits a periodic pattern with respect to the resonance frequencies of the enclosure (the four resonance frequencies are marked by dotted lines in the figure). Taking the 3Hz bandwidth curve as an example, Δf takes a smaller value when the targeted narrowband is far from the resonance frequencies of the enclosure, suggesting that the resonator should be tuned to a frequency approximately equal or very close to the central frequency of the targeted narrowband noise for maximum noise reduction. Δf increases when the targeted band approaches one of the resonance frequencies of the enclosure, indicating a better control performance of a mistuned resonator than a tuned one. The maximum Δf, however, occurs at the frequency slightly away from the resonance frequencies of the enclosure. The phenomenon can be explained by observing the control effect of the resonator shown in Fig. 4, in which, with a tuned resonator, the SPL experiences a decrease over part of the bandwidth and an increase over the other part, resulting in a neutralized band-averaged energy reduction. To avoid this, the resonator has to be mistuned away from the central

frequency of the noise to achieve a reduction in the SPL within the 3Hz bandwidth. After passing the maximum, Δf drastically drops to a relatively small value before starting the next cycle. If the targeted band becomes broader, it can be observed that although the three curves follow similar variation trend, they are different in terms of the amplitude. In general, a wider frequency band requires a larger degree of mistuning.

To examine the differences in the performance of the tuned resonator and optimally tuned resonator, a band-averaged energy reduction difference ΔER is defined as

$$\Delta\text{ER} = \text{ER}_{optimal} - \text{ER}_{tuned} \,, \tag{21}$$

where $\text{ER}_{optimal}$ and ER_{tuned} are the energy reduction (ER) value achieved by the optimally tuned resonator and the tuned resonator, respectively. As observed in Fig. 6(b), the variation trends of the ΔER are similar to that of Δf. Near resonance frequencies, a mistuned resonator is clearly more preferable to a tuned one. The largest ΔER which can be achieved in the present case can be as high as 8dB, nearly twice as much as that achieved by the tuned resonator. However, it is noted that the benefit of using an optimally tuned resonator becomes less obvious when the frequency band enlarges, as evidenced by the decrease in ΔER with the increase of the bandwidth, shown in Fig. 6(b).
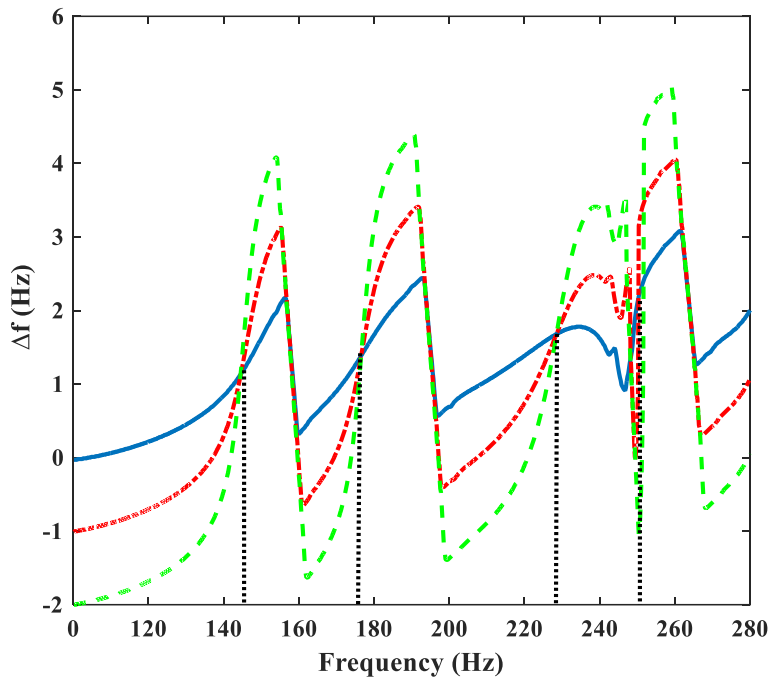
(a)
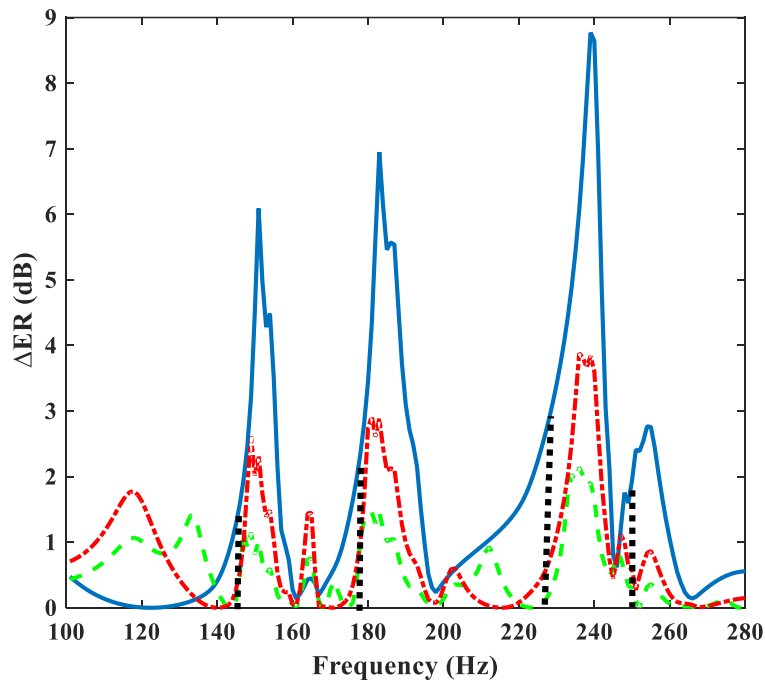
(b)

Fig. 6. (a) Difference in Helmholtz frequency between an optimally tuned and a tuned resonator as a function of the central frequency of a narrowband noise; (b) Difference in energy reduction

between an optimally tuned and a tuned resonator as a function of the central frequency of a narrowband noise. Targeted bandwidth: —— 3Hz; -·-·-·- 5Hz; ----- 7Hz.

The mistuning effect is a result of the coupling between the resonator and multiple modes of the enclosure, as opposed to the ideal case in which the resonator is assumed to be coupled to a single enclosure mode. For the latter case, Fahy and Schofield [12] suggests that the best performance occurs when the resonator is tuned to the resonance frequency of the enclosure. Figures 7(a) and 7(b) show Δf as a function of the number of the enclosure modes used in the simulation, for a 3Hz bandwidth narrowband noise, centered at 176.6Hz and 205Hz, respectively. The enclosure modes on the *x*-axis are arranged according to their closeness to the central frequency of the narrowband noise. It can be observed in Fig. 7(a) and 7(b) that Δf converges only when a sufficient number of enclosure modes are considered. For the control of a narrowband noise in this frequency region, the resonator generates an acoustic field to oppose to the primary acoustic field. The resultant acoustic field in the enclosure, instead of being dominated by a single enclosure mode, involves multiple modes of the enclosure, thus requiring a tuning strategy different from that of the ideal case in which the enclosure is assumed to be dominated a single mode. Particularly in Fig. 7(a), where the narrowband noise is centered at the resonance frequency of the enclosure, Δf is zero when only one mode is considered, in agreement with the conclusion of Fahy and Schofield [12].
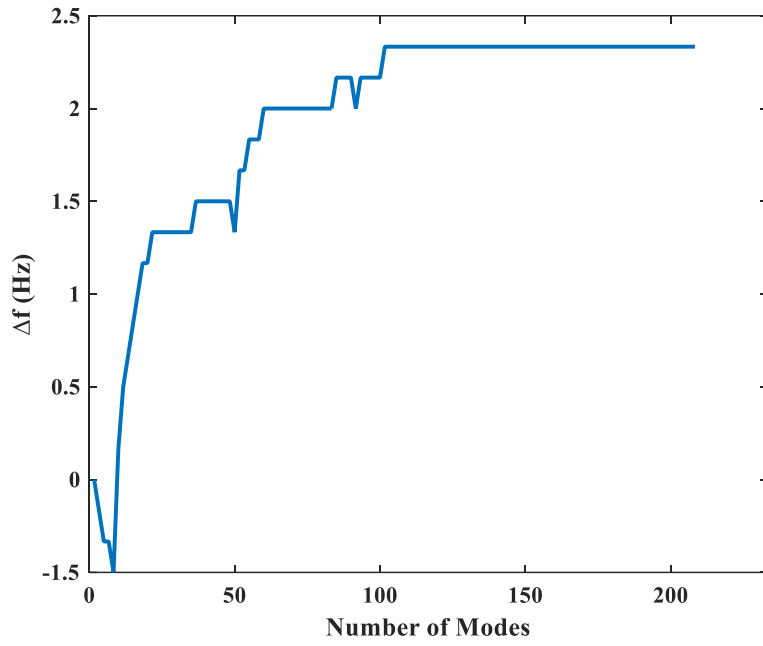
(a)
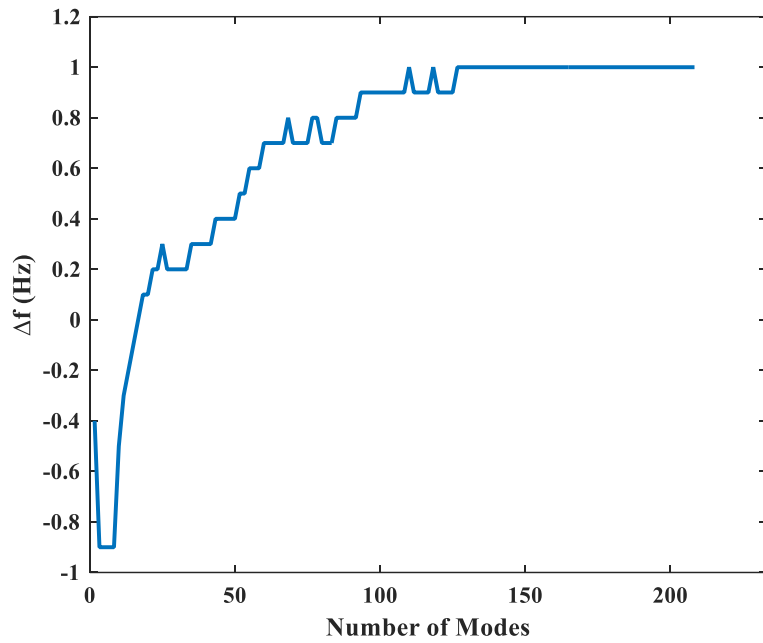
(b)

Fig. 7. Effect of the modal coupling on Δf with a 3Hz bandwidth centered at: (a) 176.6Hz, (b) 205Hz.

## 4. Tuning of the internal resistance of the resonators

The resonator internal resistance is another important parameter affecting the noise reduction mechanism. Note that a tuning of the acoustic resistance of resonators leads to a change in its damping which subsequently affect the phase on the frequency response function curves in the vicinity of the system resonances. It was found that, at a resonance frequency, the energy radiation dominates the interaction process when the target band is narrow, while it transits to an energy dissipation domination as the target band becomes wider [1]. In what follows, this issue is revisited in a much broader context to cover different frequency regions.

4.1 Off-resonance region

A 3Hz bandwidth centered at 195Hz, which is in an off-resonance region, is first investigated. Figures 8(a)-(c) show the band-averaged dissipated energy, radiated energy from the resonator and the corresponding ER when the internal resistance of the resonator is varied from 0.01 to 50 mks Rayls. A maximum ER reduction of 1.9 dB is observed in Fig. 8(c) when $R_i = 0.01$ mks Rayls, which can be referred to as the optimal resonator resistance. A similar variation trend is observed in Fig. 8(b), indicating that the noise reduction process is dominated by the resonator radiation in the present case. Despite the dominance of the radiation effect of the resonator in both the resonance and off-resonance regions, the energy radiated by the resonator in the present case is found to be smaller than that in the resonance region. In the present case, the energy radiated by the resonator is 9470 J, which is approximately half of that in a same bandwidth centered at a resonance frequency, and the dissipated energy is around 20% of its counterpart [15].
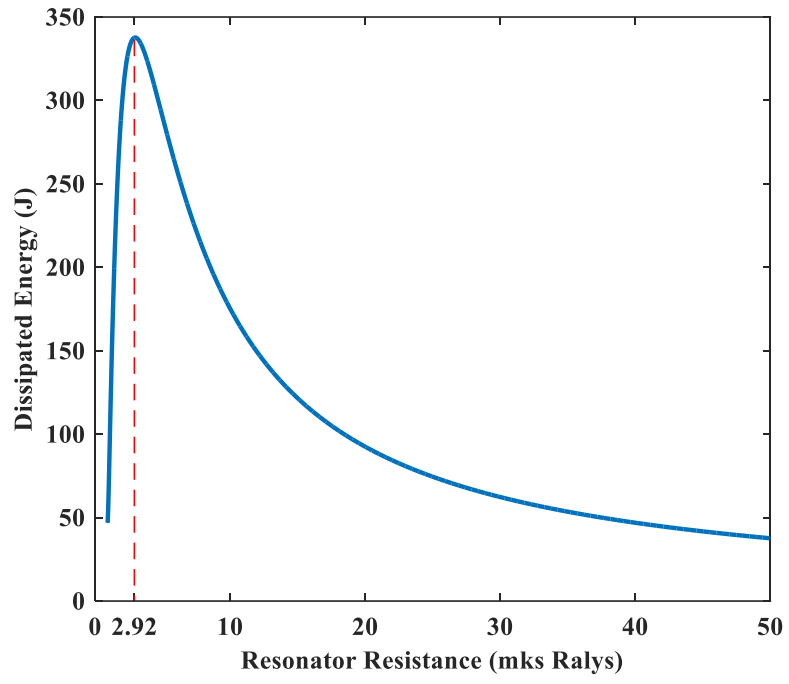
(a)
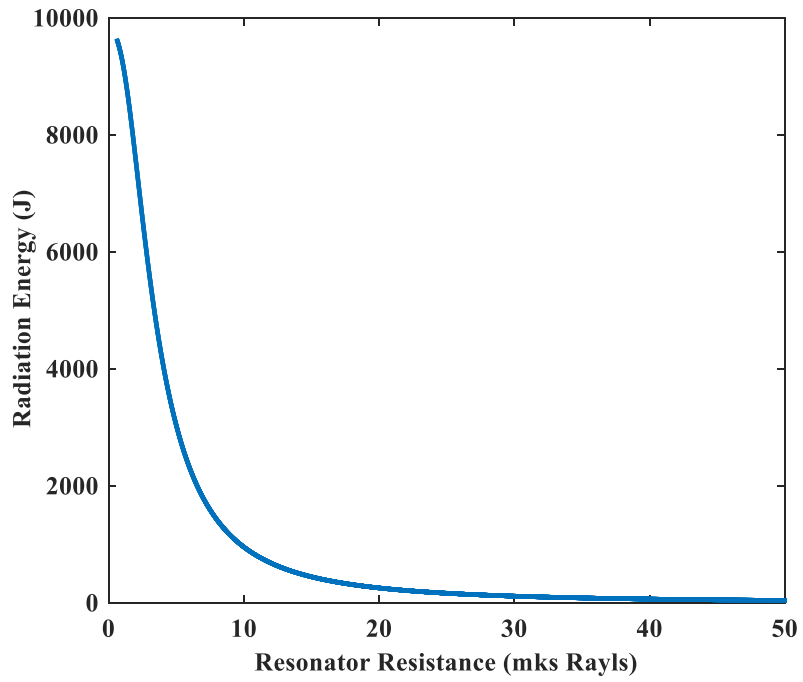
(b)
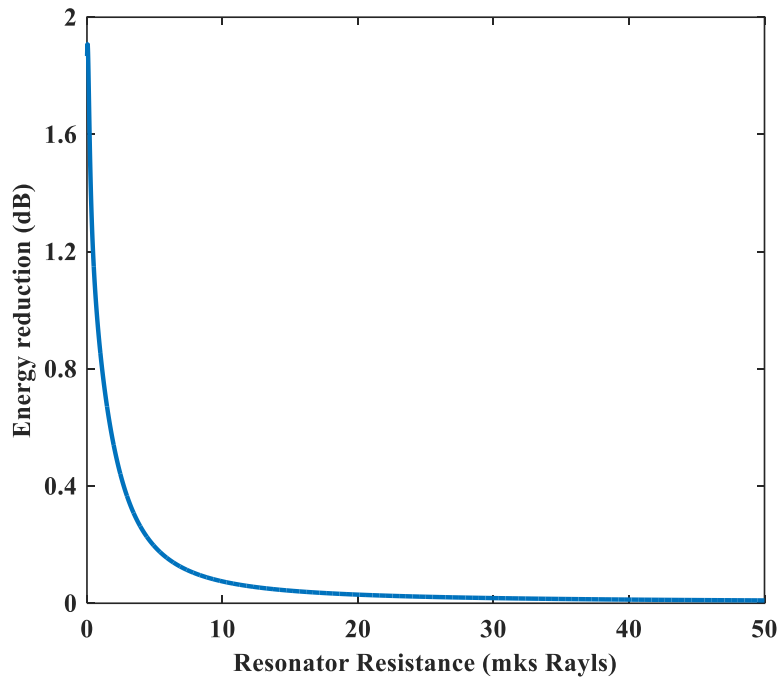
(c)

Figure 8. 3Hz bandwidth centered at 195Hz: (a) Energy dissipated by the resonator; (b) Energy radiated by the resonator; (c) Energy Reduction in the enclosure

Analyses are then conducted for different bandwidths centered at 195Hz. The bandwidth varies from 0.2Hz to 10Hz. For each frequency band, two optimal internal resistances of the resonator are calculated. One is obtained by maximizing the ER and denoted as the optimal resistance R_{opt}. The other one is obtained by maximizing the energy dissipation by the resonator and denoted as R_{dis}. The comparison between R_{opt} and R_{dis} in terms of the bandwidth is shown in Fig. 9. It is observed that R_{opt} remains small as the bandwidth increases, suggesting that the noise reduction in the enclosure is dominated by the radiation effect of the resonator and this working mechanism is independent of the bandwidth of interest.
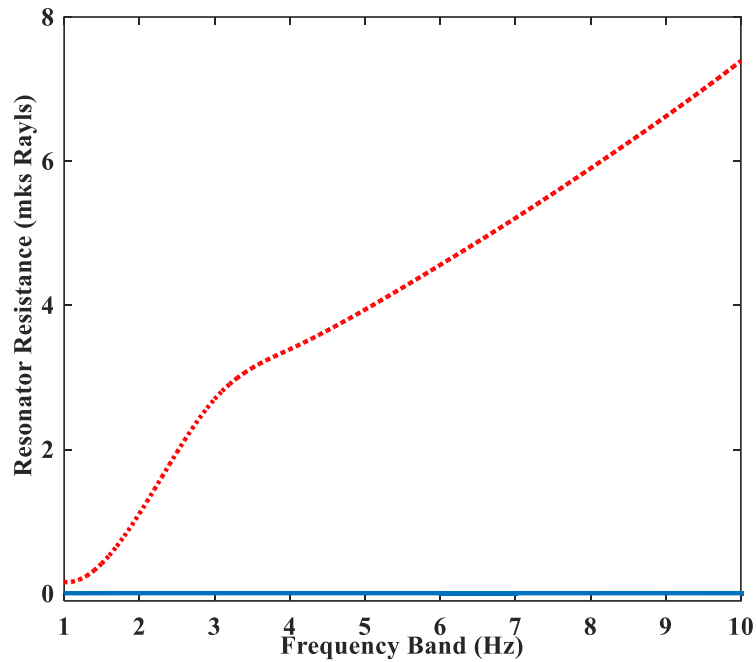
(a)

Figure 9. Effect of the bandwidth on the optimal resistance at center frequency 195Hz: — optimal resistance for maximum ER; - - - resistance for maximum energy dissipation.

To depict the overall picture of the working mechanism of the resonator across different frequency regions, the optimal resistance for ER has been calculated for different central frequencies from 170Hz to 235Hz, across two resonance frequencies 176.6Hz and 228.4Hz. Results are shown in Fig. 11 for different bandwidths. For each frequency band that is analyzed, the optimal resistance is obtained based on the optimally tuned resonator so as to develop a systematic design strategy, with which the two most important parameters of the resonator, the Helmholtz frequency and the internal resistance, can be taken into account simultaneously.

It can be seen in Fig. 10 that the optimal internal resistance of the resonator undergoes different variations in two typical frequency regions: resonance and off-resonance regions as defined previously. In the resonance region, the bandwidth excises an obvious influence on the optimal values of the resistance. The optimal resistance takes small values when the frequency band is very narrow (3Hz), demonstrating the dominance of sound radiation from the resonator in this case. It then undergoes obvious increases when the bandwidth is increased (to 5Hz)

before losing the momentum when the bandwidth becomes larger (above 5Hz). Within this resonance region, the resonator needs to be strongly coupled to the dominating resonance mode to ensure an effective noise reduction, which is sensitive to the internal resistance of the resonator. Changes in the optimal internal resistance of the resonator reflects the balance that needs to be stricken between the sound radiation and the energy dissipation of the resonator in order to achieve the maximum sound reduction in the enclosure. In the off-resonance region, the optimal internal resistance is kept low and not sensitive to the bandwidth, indicating the dominant radiation effect produced by the resonator.
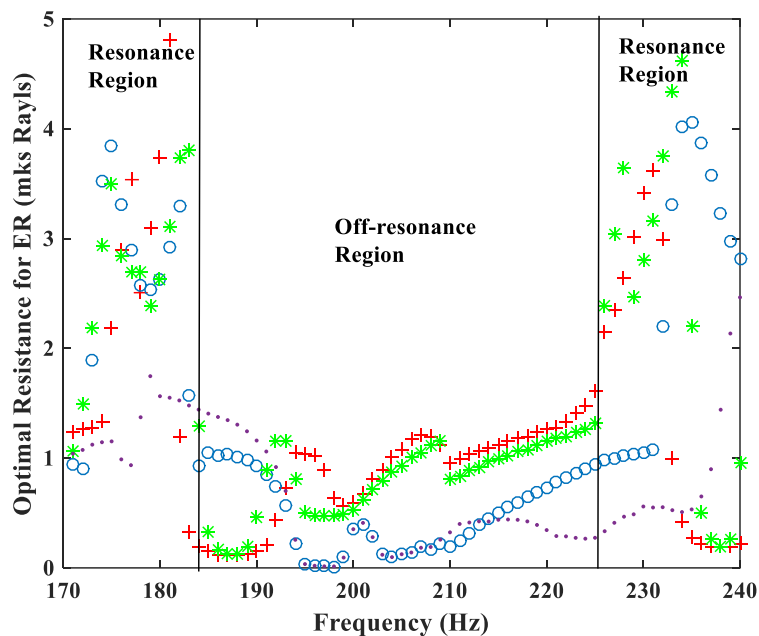

Figure 10. Optimal resistance for varied central frequency and bandwidth considering the mistuning effect. Bandwidth: · 3Hz; ∗ 5Hz; ○ 7Hz; + 15Hz.

5. Experiment Validations

The proposed design strategy is validated using a multi-cavity system, which consists two sub-cavities as shown in Fig. 11(a). The system was investigated as a simplified model of a spacecraft cabin module. The cavity wall is made of 30mm thick acrylic panels and can be considered acoustically rigid. Two circular holes are drilled at (0, 50, 75) mm and (710, 400, 150) mm in sub-cavity 1, used to connect to a loudspeaker to excite the primary sound field in

the enclosure and to pass the wires of the measurement microphones, respectively. Two

microphones are installed at (10, 50, 750) mm and (830, 150, 250) mm in sub-cavity 1. The

measured quantity is the transfer function of the acoustic pressure measured at two microphone

positions [18, 19]. The transfer function of the empty cavity without resonator is shown in

Fig. 11(b). The resonators used in the experiments are T-shaped acoustic resonators. A method

to characterize the detailed properties of the T-shaped acoustic resonator is documented in [20].
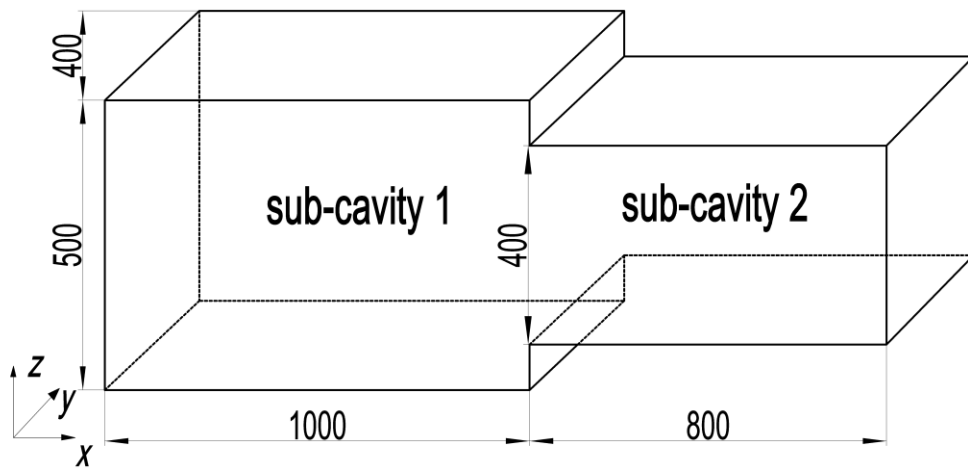
(a)
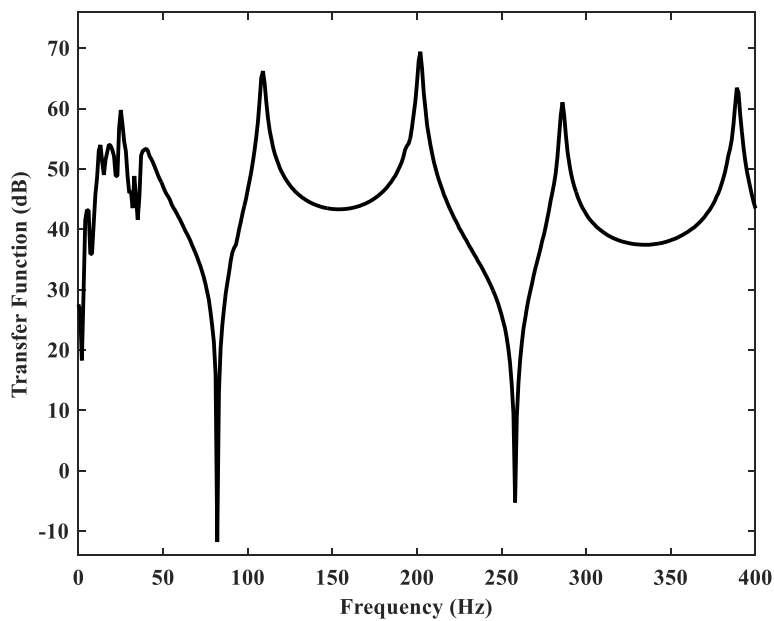
(b)

Fig. 11 (a) Experimental acoustic cavity configurations; (b) Transfer function of the acoustic pressure measured at two microphone positions without resonator.

Two frequency bands [190, 195] Hz and [325, 330] Hz with a 5Hz bandwidth are considered, the former being close to the resonance frequency 202Hz and the latter is relatively far from any resonance frequencies of the system. The configurations and detailed dimensions of the T-shaped resonator are shown in Fig. 12 and Tab. 2, respectively.
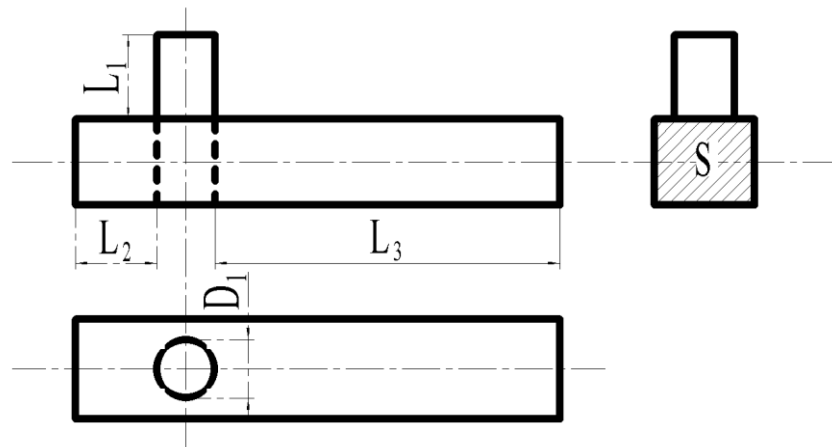

Fig. 12 Configurations of the T-shaped resonator

Table 2 Physical dimensions of the T-shaped resonator

Resonator	Helmholtz Frequency (Hz)	D_1 (mm)	S (mm)	L_1 (mm)	L_2 (mm)	L_3 (mm)
TAR_189	189	21	30x30	19	19	405
TAR_192.5	192.5	21	30x30	19	19	397
TAR_328	328	21	30x30	19	19	214

For the frequency band [190, 195] Hz with a central frequency at 192.5Hz, the control performances using two resonators located at (768, 155, 39) mm inside sub-cavity 2 are compared. The two resonators, denoted by TAR_192.5 and TAR_189 and shown in Fig.13(b), have their Helmholtz frequencies at 192.5Hz and 189Hz, respectively. Control results are shown in Fig. 13(a). It can be seen that the tuned resonator TAR_192.5 fails to reduce the SPL within the target frequency band. However, the mistuned resonator TAR_189 achieves an approximately 9dB ER within the target frequency band, in agreement with the theoretical

analyses. It also confirms the fact that a mistuned resonator with a negative Δf is necessary in this case, in agreement with the previous numerical analyses as well. As for the other frequency band [325, 330] Hz using TAR_328, shown in Fig. 14(b) and located at the same point inside sub-cavity 2, Fig. 14(a) shows a 1.4 dB SPL reduction within the frequency band of interest, in agreement with the theoretical analyses that no mistuning is needed in this case.
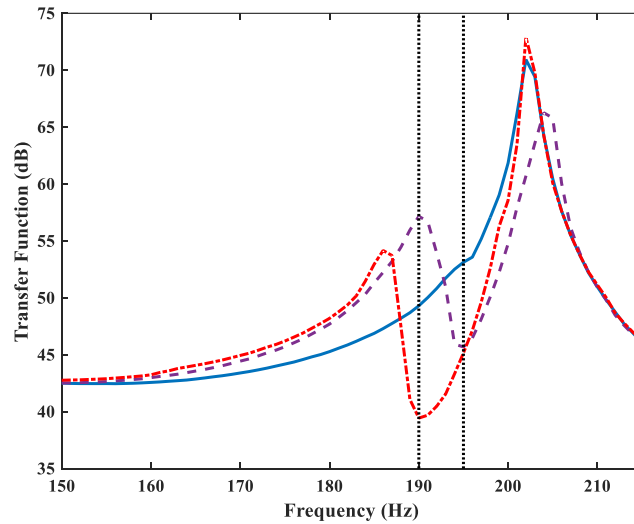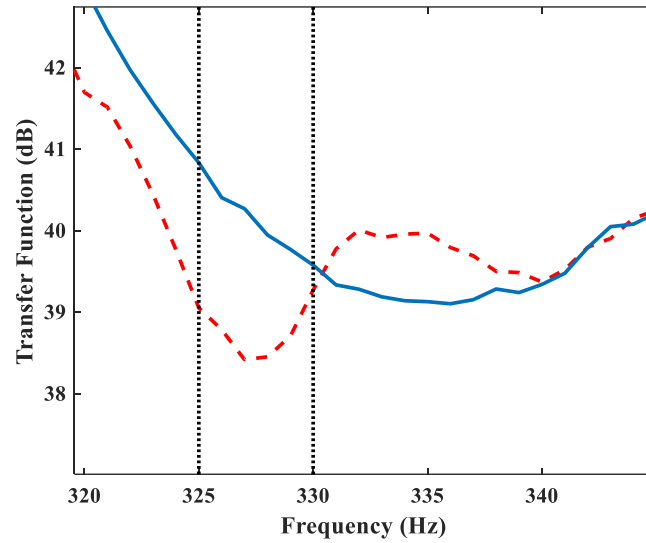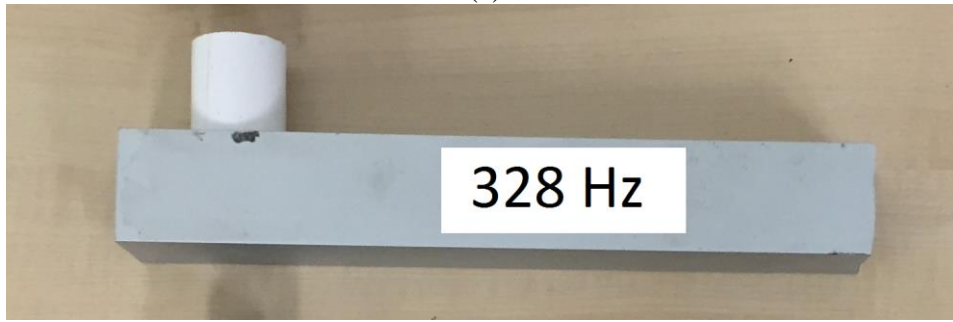

(a)

(b)

Fig. 13. (a) SPL control with T-shaped acoustic resonator within [190, 195] Hz: —— no resonator; -·-·- with TAR_189; ---- with TAR 192.5. (b) TAR_189 and TAR_192.5.

Fig. 14. (a) SPL control with T-shaped acoustic resonator within [325, 330] Hz: ——— no resonator; ----- with TAR_328. (b) TAR_328.

6. Conclusions

Based on an analytical development of an acoustic enclosure coupled with a Helmholtz resonator, a tuning strategy in terms of Helmholtz frequency and internal resistance is developed. Main conclusions are summarized as follows:

(1) Noise reduction can be maximized through an optimal tuning of the resonators, with their Helmholtz frequency mistuned from the central frequency of the targeted frequency band. The mistuning effect arises as a result of the multi-modal coupling within the enclosure-resonator system. The optimal mistuning level Δf, either positive or negative, depends on frequency regions. In the resonance region, Δf, albeit small, should be carefully

determined due to the high sensitivity of the sound filed to the resonator. In the off-resonance region, mistuning effect is insignificant. In the transition region, optimal Δf can take a large value, which should be meticulously determined through numerical simulations. As a general rule, same extra care is needed in dealing with narrow-band noise control.

(2) The optimal tuning of the internal resistance of the resonators depends on the targeted frequency region and the bandwidth. Within the resonance region, the optimal internal resistance should increase with the bandwidth. In the transition and off-resonance regions, only narrow band noise reduction (typically smaller than 5Hz) can be achieved by using resonators with a low internal resistance, as a result of enhanced radiation effect of the resonators.

Reference

[1] Rayleigh, *The theory of sound*. Vol. 2. 1896, Macmillan.

[2] S. Kim, Y.H. Kim, and J.H. Jang, "A theoretical model to predict the low-frequency sound absorption of a Helmholtz resonator array,″ J Acoust Soc Am **119**(4), 1933-1936 (2006).

[3] J.M. Mason and F.J. Fahy, "The use of acoustically tuned resonators to improve the sound transmission loss of double-panel partitions,″ J sound Vib **124**(2), 367-379 (1988).

[4] Q. Mao and S. Pietrzko, "Experimental study for control of sound transmission through double glazed window using optimally tuned Helmholtz resonators,″ Appl Acoust **71**(1), 32-38 (2010).

[5] R.C. Chanaud, "Effects of geometry on the resonance fequency of helmholtz resonator,″ J sound Vib **178**(3), 337-348 (1994).

[6] U. Ingard, "On the Theory and Design of Acoustic Resonators,″ J Acoust Soc Am **25**(6), 1037-1061 (1953).

[7] M. Alster, "Improved calculation of resonant frequencies of Helmholtz resonators," J sound Vib **24**(1), 63-85 (1972).

[8] R.L. Panton and J.M. Miller, "Resonant frequencies of cylindrical Helmholtz resonators," J Acoust Soc Am **57**(6), 1533-1535 (1975).

[9] J.M. Coulon, N. Atalla, and A. Desrochers, "Optimization of concentric array resonators for wide band noise reduction," Appl Acoust **113**(1), 109-115 (2016).

[10] S.J. Estève and M.E. Johnson, "Reduction of sound transmission into a circular cylindrical shell using distributed vibration absorbers and Helmholtz resonators," J Acoust Soc Am **112**(6), 2840-2848 (2002).

[11] F.J. Van Leeuwen, "The damping of eigentones in small rooms by helmholtz resonators," European Broadcasting Union Review, A-Technical **62,** 155-161 (1960).

[12] F.J. Fahy and C. Scofield, "A note on the interaction between a Helmholtz resonator and an acoustic mode of an enclosure," J sound Vib **72**(3), 365-378 (1980).

[13] A. Cummings, "The effects of a resonator array on the sound field in a cavity," J sound Vib **154**(1), 25-44 (1992).

[14] D. Li and L. Cheng, "Acoustically coupled model of an enclosure and a Helmholtz resonator array," J sound Vib **305**(1), 272-288 (2007).

[15] G. Yu, D. Li, and L. Cheng, "Effect of internal resistance of a Helmholtz resonator on acoustic energy reduction in enclosures," J Acoust Soc Am **124**(6), 3534-3543 (2008).

[16] L.E. Kinsler, A.R. Frey, A.B. Coppens, J.V. Sanders, *Fundamentals of acoustics*, 4th Edition. Wiley, (1999).

[17] D. Li, L. Cheng, G. Yu, and J. S. Vipperman, "Noise control in enclosures: modeling and experiments with T-shaped acoustic resonators," J Acoust Soc Am **122**(5), 2615-2625 (2007).

[18] C. Yang, L. Cheng, and Z. Hu, "Reducing interior noise in a cylinder using micro-perforated panels," Appl Acoust **95**, 50-56 (2015).

[19] C. Yang and L. Cheng, "Sound absorption of microperforated panels inside compact acoustic enclosures," J sound Vib **360**, 140-155 (2016).

[20] G. Yu and L. Cheng, "Location optimization of a long T-shaped acoustic resonator array in noise control of enclosures," J sound Vib **328**(1), 42-56 (2009).